Conf-751016--4

DP-MS-75-86

MASTER

NEUTRON RADIOGRAPHIC DETECTION LIMITS OF FLUIDS IN METAL PIPES

by

W. G. Winn

Savannah River Laboratory
E. I. du Pont de Nemours & Co.
Aiken, South Carolina 29801

NOTICE

This report was prepared as an account of work sponsored by the United States Government. Neither the United States nor the United States Energy Research and Development Administration, nor any of their employees, nor any of their contractors, subcontractors, or their employees, makes any warranty, express or implied, or assumes any legal liability or responsibility for the accuracy, completeness or usefulness of any information, apparatus, product or process disclosed, or represents that its use would not infringe privately owned rights.

A Paper for Presentation at
1975 National Conference
American Society for Nondestructive Testing
Atlanta, Georgia
October 13-16, 1975

This paper was prepared in connection with work under Contract No. AT(07-2)-1 with the U. S. Energy Research and Development Administration. By acceptance of this paper, the publisher and/or recipient acknowledges the U. S. Government's right to retain a nonexclusive, royalty-free license in and to any copyright covering this paper, along with the right to reproduce and to authorize others to reproduce all or part of the copyrighted paper.

DISTRIBUTION OF THIS DOCUMENT IS UNLIMITED

DISCLAIMER

This report was prepared as an account of work sponsored by an agency of the United States Government. Neither the United States Government nor any agency Thereof, nor any of their employees, makes any warranty, express or implied, or assumes any legal liability or responsibility for the accuracy, completeness, or usefulness of any information, apparatus, product, or process disclosed, or represents that its use would not infringe privately owned rights. Reference herein to any specific commercial product, process, or service by trade name, trademark, manufacturer, or otherwise does not necessarily constitute or imply its endorsement, recommendation, or favoring by the United States Government or any agency thereof. The views and opinions of authors expressed herein do not necessarily state or reflect those of the United States Government or any agency thereof.

DISCLAIMER

Portions of this document may be illegible in electronic image products. Images are produced from the best available original document.

NEUTRON RADIOGRAPHIC DETECTION LIMITS OF FLUIDS IN METAL PIPES

by

W. G. Winn

Savannah River Laboratory
E. I. du Pont de Nemours & Co.
Aiken, South Carolina 29801

ABSTRACT

Thermal neutron radiography has been used to image thin films of various fluids in thick-walled high-pressure process pipes. A 3.5×10^6 n/(cm^2-sec) thermal neutron beam and standard transfer imaging techniques were used to provide radiographs of the fluid-bearing pipes. In addition, a computer graphics procedure was developed which simulated the neutron radiographs; this method permitted examination of some fluid-pipe configurations not studied experimentally. Actual pipe outer diameters ranged from 1/4 to 9/16 in. (OD/ID = 3), but the graphics method was used for some cases outside this range.

Fluids in the thermal cross section range $0.29\ cm^{-1} \leq \Sigma^f_{th} \leq 3.47\ cm^{-1}$ were examined for pipes with $0.099\ cm^{-1} \leq \Sigma^p_{th} \leq 1.15\ cm^{-1}$. For $\Sigma^f_{th} > \Sigma^p_{th}$, the smallest measured film thickness t_s varied 0.006 to 0.040 in. with decreasing Σ^f_{th}; a semiempirical model described $t_s = t_r + t_a$, where t_r corresponded to resolution and t_a depended on the bulk attenuation strength of the fluid.

For $\Sigma_{th}^{f} < \Sigma_{th}^{p}$, part of the fluid film t_m was masked by the pipe. The calculated physical film thickness $t_p = t_a + t_m$ ranged from 0.003 to 0.035 in. for smallest detected fluid films. Detection of low Σ_{th} fluids was improved as much as 60% when the pipes were tilted 60° toward the neutron beam. Other options for improved detection were investigated using simulated radiographs.

INTRODUCTION

Routine maintenance of process pipes at the Savannah River Plant has indicated that undesirable fluids can build up in the various gas lines. Neutron radiography was evaluated as a means for establishing the presence or absence of the fluid contaminants to avoid the cumbersome routine of removing pipe sections for fluid contaminant inspection. Neutron radiography appeared to have a decided advantage over X-radiography due to the large atomic number of the pipe material. At the outset of the present work, thin fluid films within the pipes were considered the most difficult geometry of fluid to image. Although neutron radiographic studies of reactor fuel elements[1-8] have yielded information related to the imageability of concentric annular objects, a survey of the literature indicated a paucity of neutron radiographic studies for geometries describing fluid films within pipes. However, the detection of water films contained within planar channels has been examined.[9]

Neutron radiographs of the fluid-bearing pipes were produced using the Standard Pile (SP) reactor at the Savannah River Laboratory. A computer graphics approach for simulating radiographs was used to assist in experimental design and to examine some fluid-pipe configurations that were not studied experimentally. It is anticipated that these preliminary evaluations will be

supplemented by a later study with a portable neutron radiography facility having a ^{252}Cf neutron source.

DETECTION OF FLUID FILMS IN PIPES

Neutron radiographic detection of fluid films in pipes is most efficient when the neutron beam is attenuated by the maximum available thickness of fluid, as indicated in Figure 1. A minimum thickness t_a of fluid film is required to produce a detectable image on the radiograph. The corresponding smallest film thickness t_s registered on the radiograph will be given by

$$t_s = t_r + t_a \tag{1}$$

where t_r is the resolution.

When the thermal neutron cross section of the pipe (Σ^p_{th}) is noticeably larger than that of the fluid (Σ^f_{th}), the pipe can mask a thickness t_m of the fluid film in the radiograph. Figure 2 illustrates this feature for D_2O in stainless steel pipes; the additional attenuation by D_2O near the tangent edge of the pipe cavity is only a small fraction of the attenuation by the empty pipe. Thus, when $\Sigma^p_{th} > \Sigma^f_{th}$, a detected fluid film of thickness t_a implies that the physical thickness of the fluid is

$$t_p = t_a + t_m \tag{2}$$

Analytic expressions for t_r, t_a, and t_m may be approximated for cases in which the pipe and foil are irradiated both under normal neutron beam incidence and when they are tilted at an angle θ toward the neutron beam. At angle θ, the fluid is

projected more thickly into the neutron beam, allowing better detectability at the expense of resolution.

The thin film resolution was approximated as

$$t_r = 2\ R_o \sec\theta \tan\phi \qquad (3)$$

where the parameters are defined in Figure 1a and b. Minimum detectable thickness t_a of the fluid film was considered to be related to the neutron removal capability C of the entire film. Referring to Figure 1c, C is defined as

$$C = \int_o^{t_a} (\Sigma_{th}^f\ \ell)\ dZ = 4/3\ \Sigma_{th}^f\ \sqrt{2R_1\ t_a^3}$$

Assuming C to be a constant for all minimally detectable fluid films,

$$t_a = A\ (\Sigma_{th}^f)^{-2/3}\ R_1^{-1/3}$$

where $A = (3/4\ C)^{2/3}$. The above case is generalized to cases for pipes tilted by θ by replacing Σ_{th}^f with $\Sigma_{th}^f \sec\theta$, viz.

$$t_a = A(\Sigma_{th}^f \sec\theta)^{-2/3}\ R_1^{-1/3} \qquad (4)$$

Utilizing Equations (1), (3), and (4), a semiempirical expression for t_s is

$$t_s = 2\ R_o \sec\theta \tan\phi + A\ (\Sigma_{th}^f \sec\theta)^{-2/3}\ R_1^{-1/3} \qquad (5)$$

The masking parameter t_m for pipes of similar geometry (OD/ID) increases with R_o and is noticeable for fluids with $\Sigma_{th}^f << \Sigma_{th}^p$. Accordingly, it was assumed that

$$t_m = NM\ R_o\ (\Sigma_{th}^p - \Sigma_{th}^f) \sec\theta \qquad (6)$$

where the constant M is determined experimentally for a given pipe geometry, and N is 0 or 1 for $\Sigma_{th}^{f} \geq$ or $\leq \Sigma_{th}^{p}$. The factor sec θ corrects the attenuation thickness for the tilted case. Using Equations (2), (4), and (6), a semiempirical expression for the smallest thickness of film detectable is

$$t_p = A(\Sigma_{th}^{f} \sec \theta)^{-2/3} R_1^{-1/3} + NM R_o (\Sigma_{th}^{p} - \Sigma_{th}^{f}) \sec \theta \quad (7)$$

EXPERIMENTAL TECHNIQUES

The transfer method utilized in these studies was similar to that described in earlier work at this laboratory.[10] The essentials of the experimental arrangement are shown in Figure 3, where a collimated beam of thermal neutrons [3.5×10^6/(cm^2-sec)] imaged the fluid-bearing pipes on 10-mil dysprosium foils directly behind the pipes. After sample irradiations of 4 to 8 minutes, the foils were placed in a lighttight cassette where they exposed either *Kodak** AA or *Kodak* $NS_{54}T$ X-ray film for 15 to 60% of the ^{165}Dy (140 min) decay. The exposed X-ray film was then developed using standard procedures.

Neutron radiographs were taken of aluminum and/or stainless steel pipes containing graphite, heavy water, carbon tetrachloride, water, and two types of oil. Relatively thick-walled pipes (OD/ID = 3) of various sizes (OD = 1/4, 3/8, and 9/16 in.) were examined. In many cases, aluminum wedges were inserted in the fluids to define film geometries. Conical wedges were used to

---

* *Kodak* is a trademark of Eastman Kodak Co.

define families of annular films, and truncated cylindrical wedges defined families of trough-like films. To determine whether image contrast for weakly imaged fluids could be improved, some neutron radiographs were obtained with the pipes orientated 60° toward the neutron beam.

Examination of these radiographs under X5 magnification permitted measurement of many fluid film thicknesses as accurately as ±2 mil; however, for weakly attenuating fluids ($\Sigma_{th}^{f} < 0.5\ cm^{-1}$) the poor contrast between the film and background pipe yielded uncertainties as large as ±15 mil. Accurate measurements of annular objects are best obtained using a microdensitometer,[1-3] but the randomness of fluid film locations in anticipated applications suggested that detection by visual means would be more practical for the present studies. Later implementation of an electronic image analyzer utilizing a scanning microdensitometer might automate the detection procedures.[4]

A summary of details concerning the pipe and fluid materials examined and a figure reference guide for the corresponding radiographs is given in Table I.

COMPUTER GRAPHICS TECHNIQUE

Simulated neutron radiographs were produced by the DISSPLA[11] graphics routine implemented on the IBM 360-195 computer at the Savannah River Laboratory. Straight lines were drawn parallel to the pipe axes by the code and were spaced to represent the darkening expected for a particular fluid-pipe radiographic image.

The simulated radiographs agreed reasonably well with actual cases when P, the parallel line density, was given by

$$P = ae^{-\int \Sigma_{th} dx}$$

where a is a constant, Σ_{th} is the total thermal neutron cross section, and the exponential factor represents the attenuation for 0.0253 eV neutrons that traverse a fluid-pipe thickness $\int dx$. Comparisons between actual and simulated neutron radiographs are presented in Figures 4 through 7. The simulated radiographs are photographic enlargements obtained directly from microfiche negatives produced by DISSPLA.

Simulated radiographs were produced for conical and trough-like fluid films similar to those obtained experimentally. In addition, lead and copper pipe configurations were examined. Moreover, the detectability of pure tritiated water (T_2O) in a variety of pipes was studied. With the exception of T_2O, all Σ_{th} values for pipes and fluids were obtained from Reference 12. In the case of T_2O, a value of $\Sigma_{th} = 0.28\ cm^{-1}$ was estimated utilizing scattering amplitudes[13] for T and cross section data[12] for O, while estimating the molecular binding enhancement of Σ_{th} (T_2O) by comparison with Σ_{th} (H_2O) and Σ_{th} (D_2O). A summary of the simulated radiographs and a figure reference guide are included in Table I.

ANALYSIS OF RESULTS

Examination of t_s

Measured values of t_s are presented in Table II for a variety of experimental cases. These values were used to examine Equation (5), which may be written

$$y = Ax + 2 \tan \phi$$

Values of $y = t_s (R_o \sec \theta)^{-1}$ and $x = (\Sigma_{th}^f \sec \theta)^{-2/3} R_1^{-1/3} (R_o \sec \theta)^{-1}$ are plotted in Figure 8. The resulting straight line with $A = 5.0$ mil $cm^{-2/3}$ $in.^{+1/3}$ and $2 \tan \phi = 16.0$ mil/in. illustrates the self-consistency of Equation (5) for describing t_s (mil). Values of t_s calculated with this formalism are included in Table II.

The above results also permit examination of Equation (3) for t_r. The dependence of t_r on $R_o \sec \theta$ is confirmed in Figure 8, and the $2 \tan \phi$ factor may be compared with the experimental beam geometry. Using Figure 3, $L/D = 53.0$ is compared with $(2 \tan \phi)^{-1} = 0.0625$ in./mil $= 62.5$. The agreement is satisfactory and implies that t_a given by Equation (4) is also reasonable. Calculated values for t_r and t_a are included in Table II.

Examination of t_p

Values of t_p with $t_m = 0$ are presented in Table II. The masking parameter t_m must be known to estimate t_p in general.

Values of t_m were estimated using the radiographs of oils in stainless steel pipes. The oils appeared to penetrate $t_m \sim 30 R_o$ mil into the interior wall of the pipe where R_o is given in

inches. (In reality, the empty portion of the pipe is masked near the tangent edge, causing the pipe cavity to appear smaller in the radiograph.) Using the above t_m in Equation (5) with $\Sigma^p_{th} = 1.15\ cm^{-1}$, $\Sigma^f_{th} = 0.0\ cm^{-1}$, and N = 1, M was calculated to be ∿25 mil-cm/in.

Using the experimentally determined values of A and M in Equation 7, the smallest thickness t_p of detectable fluid film was

$$t_p = (5.0)(\Sigma^f_{th} \sec\theta)^{-2/3} R_1^{-1/3} + 25N\, R_o\, (\Sigma^p_{th} - \Sigma^f_{th}) \sec\theta$$

Values of t_p are given for various cases where masking is present in Table III. Masking tends to nullify some of the advantage gained by tilting the pipes.

DISCUSSION AND CONCLUSIONS

General

This study demonstrated that many common industrial fluids such as H_2O, oils, and CCl_4 may be detected in thick-walled process pipes, even when distributed in thin (3-10 mil) fluid films. By contrast, low Σ_{th} fluids (D_2O and T_2O) could be detected only for much thicker films. The smallest imaged fluid film of thickness ($t_s = t_a + t_r$) could be used to infer the physical thickness ($t_p = t_a + t_m$) of the smallest detected film. While semiempirical formulae [Equations (3) and (4)] for t_r and t_a agreed satisfactorily with experimental measurements, Equation (6) for the masking parameter t_m was difficult to

appraise by measurement. As t_m is noticeably smaller than t_p, no serious error in t_p is expected.

The semiempirical expressions for t_r, t_a, and t_m appear reasonable in general; but the constants tan ϕ, A, and M must be determined uniquely for different neutron radiography systems. The collimator design influences tan ϕ; procedures for producing and analyzing the radiographs determine the detectability parameters A and M. The constants determined in this work describe a detection capability for visual analysis of the radiographs produced with L/D = 53.0. Techniques such as image enhancement[14] could be utilized to further optimize parameters A and M, and an improved beam geometry would optimize tan ϕ.

Capabilities for Detecting Weakly Imageable Fluids

Optimum detection of weakly imageable fluid films occurred when the fluid was radiographed in tilted aluminum pipes; in some instances (Figure 4), capillarity provided additional optimization by causing the fluid to be projected more thickly in the neutron beam. Radiographs with the aluminum wedges (Figures 5 through 7) indicated that trough-like films could be imaged more sharply than annular films.

In many applications, not all of the above optimizations can be realized simultaneously. If stainless steel pipes are required, the advantages gained by tilting the pipes are not as attractive, as illustrated in Figure 9. Here T_2O is imaged in tilted stainless steel and aluminum pipes of various size. Although the fluid

is imaged better upon increasing θ in both cases, masking by the stainless steel pipes still prevents detection of the thinner films; this was not true for the aluminum pipes. Also, neutron fluence considerations detailed in the figure indicate that much longer neutron irradiations are required to take radiographs of the tilted steel pipes.

When the pipe dimensions can be altered, the choice of thin-walled tubes yields an obvious advantage. In Figure 10, the detectability of various annular fluid films in 20-mil-wall stainless steel tubes is displayed. Masking is not very noticeable in these cases.

If the pipe dimensions are fixed, optimum choice of pipe material may be available. Although aluminum yields the least masking, the simulations in Figures 5 through 7 illustrate that other materials, such as lead, may be satisfactory for some applications.

Application with Portable System

The anticipated ^{252}Cf portable system can utilize the semi-empirical formulae [Equations (3) through (7)] for film thicknesses; however, the constants tan ϕ, A, and M will have to be redetermined as they are uniquely related to experimental techniques. Each parameter must be minimized to obtain optimum detectability for thin fluid films. Reducing tan ϕ below the value used in the present studies is not anticipated for the portable system, as the corresponding tradeoff in neutron beam

intensity may be prohibitive. Reduction of A and M may be possible; however, if direct neutron radiography is used, fogging of the radiographs by gamma rays from the neutron source can increase A and M.

Data are to be obtained with a commercially available portable device for pipe and fluid samples like those studied in the present work. Should gamma ray fogging prevent the detection of weakly attenuating fluids, long exposure transfer techniques will be considered.[15] Simulated radiographs including gamma ray fogging may suggest guidelines for minimizing this background.

ACKNOWLEDGEMENTS

I wish to thank J. D. Spencer, N. P. Baumann, F. B. Christensen, P. B. Parks, and H. Berger for helpful discussion of these studies. Darkroom work by V. C. Ivey, graphics programming assistance from M. B. Stroud, and SP reactor operation by J. L. Jarriel are all gratefully acknowledged.

REFERENCES

1. L. A. Thaler, "Measurement of Capsule Heat Transfer Gaps Using Neutron Radiography," *Materials Evaluation*, Vol. XXXII, March, 1974, p. 57.

2. S. J. Basham, D. R. Grieser, and J. W. Ray, "Dimensional Measurements of Cylindrical Specimens Using Neutron Radiography," *Materials Evaluation*, Vol. XXVIII, June, 1970, P. 140.

3. D. C. Cutforth, "Dimensioning Reactor Fuel Specimens from Thermal-Neutron Radiographs," *Nuclear Technology*, Vol. XVIII, April, 1973, p. 67.

4. A. Vary and K. J. Bowles, "Application of an Electronic Image Analyzer to Dimensional Measurements from Neutron Radiographs," *Materials Evaluation*, Vol. XXXII, January, 1974, p. 7.

5. H. Berger, "The Present State of Neutron Radiography and Its Potential," *Materials Evaluation*, Vol. XXX, March, 1972, p. 55.

6. H. Berger, "Neutron Radiography," *Annual Reviews of Nuclear Sciences*, E. Segrè, ed., Annual Reviews, Inc., Palo Alto, CA, Vol. 21, 1971, p. 335-364.

7. J. W. Ray, "Neutron Radiography, A Solution in Search of Problems," *Research and Development*, Vol. 20, July, 1969, p. 18.

8. H. Berger, *Neutron Radiography*, Elsevier Publishing Co., NY, 1965.

9. R. A. Moss and A. J. Kelly, "Neutron Radiographic Study of Limiting Planar Heat Pipe Performance," *International Journal of Heat Mass Transfer*, Vol. 13, 1970, p. 491.

10. M. Brown and P. B. Parks, "Neutron Radiography in Biologic Media," *Am. J. of Roent. Radium Ther. Nucl. Med.*, Vol. CVI, July, 1969, p. 472.

11. *DISSPLA, Display Integrated Software System and Plotting Language*, Integrated Software Systems Corporation, San Diego, CA, 1971.

12. *Neutron Cross Sections*, USAEC Report BNL-325, 2nd Ed. plus supplements, Brookhaven National Laboratory, Upton, NY, 1958f.

13. R. E. Donaldson, W. Bartolini, and H. Otsuki, "Measurement of the Coherent-Scattering Amplitude of Tritium," *Physical Review C*, Vol. 5, 1972, p. 1952.

14. B. R. Hunt, D. H. Janney, and R. K. Zeigler, "Radiographic Image Enhancement by Digital Computers," *Materials Evaluation*, Vol. XXXI, January, 1973, p. 1.

15. H. Berger, "Recent Progress in Neutron Imaging," *British Journal of Non-Destructive Testing*, Vol. 10, 1968, p. 26.

TABLE I

Neutron Radiographs[a]

Pipes[c]		*Figure Numbers of Radiographs of Various Fluids, actual (simulated equivalent)*[b]					
Material	*Dimensions*[c]	H_2O	*C-Oil* (H_2O)[d]	*P-Oil* (H_2O)[e]	CCl_4 (M_2O)[f]	D_2O	$C(T_2O)$
Stainless Steel (Fe)	9/16 - 3/16	4,5	4,5	4,5	5	4,5	5,9*g*
	3/8 - 1/8	4,6	4,6	4,6	6	4,6	6,9*g*
	1/4 - 1/12	4,7	4,7	4,7	7	4,7	7,9*g*
	5/8 x 0.02	10	10	10	10	10	10*g*
	3/8 x 0.02	10	10	10	10	10	10*g*
	1/8 x 0.02	10	10	10	10	10	10*g*
Copper	9/16 - 3/16	5	5	5	5	5	5
	3/8 - 1/8	6	6	6	6	6	6
	1/4 - 1/12	7	7	7	7	7	7
Lead	9/16 - 3/16	5	5	5	5	5	5
	3/8 - 1/8	6	6	6	6	6	6
	1/4 - 1/12	7	7	7	7	7	7
Aluminum	9/16 - 3/16	5*g*	5	5*g*	5*g*	5	5*g*,9*g*
	3/8 - 1/8	6*g*	6	6*g*	6*g*	6	6*g*,9*g*
	1/4 - 1/12	7*g*	7	7*g*	7*g*	7	7*g*,9*g*

a. Each entry refers to a figure number. Underlined entries indicate that both experimental and simulated results are compared. Other numbers are for simulated cases alone.

b. Due to aluminum wedges: $\Sigma_{th}\,(CCl_4)_{eff} = \Sigma_{th}\,(CCl_4) = \Sigma_{th}(Al) = 1.17\ cm^{-1} \approx \Sigma_{th}\,(M_2O)$; $\Sigma_{th}\,(C)_{eff} = \Sigma_{th}\,(C) - \Sigma_{th}(Al) = 0.29\ cm^{-1} \approx \Sigma_{th}\,(T_2O)$.

c. Pipe dimensions in inches are given as OD-ID or OD x wall.

d. C-oil is a pump-grade compressor oil (Shell Tellus No. 15).

e. P-oil is a pump-grade piston oil (Rusher Instr. Corp. No. 55-500).

f. M_2O is a mixture of H_2O and D_2O with $\Sigma_{th} = 1.0\ cm^{-1}$.

g. Tilted pipe radiograph included.

TABLE II

Summary of Experimental Results

Fluid, actual (simulated equivalent)	*Pipe,*[a] *in.*	*Tilt, sec θ*	*Measurements* t_s, *mils*	*Calculations,*[b] *mils* t_s	t_r	$t_a = t_p$
	9/16 - 3/16	1	9 ±2	9.3	4.5	4.8
H_2O, oils		2	13 ±2	12.0	9.0	3.0
(Σ_{th} = 3.47 cm^{-1})	3/8 - 1/8	1	7 ±2	8.5	3.0	5.5
		2	9 ±2	9.5	6.0	3.5
	1/4 - 1/12	1	6 ±2	8.3	2.0	6.3
		2	8 ±2	8.0	4.0	4.0
	9/16 - 3/16	1	15 ±3	14.4	4.5	9.9
CCl_4 (M_2O)[c]		2	13 ±2	15.2	9.0	6.2
(Σ_{th} = 1.17 cm^{-1})[d]	3/8 - 1/8	1	15 ±3	14.3	3.0	11.3
		2	10 ±2	13.1	6.0	7.1
	1/4 - 1/12	1	15 ±3	15.0	2.0	13.0
		2	11 ±2	12.2	4.0	8.2
	9/16 - 3/16	1	30 ±6	29.7	4.5	25.2
C (T_2O)		2	24 ±7	24.9	9.0	15.9
(Σ_{th} = 0.29 cm^{-1})[d]	3/8 - 1/8	1	40 ±15	31.8	3.0	28.8
		2	24 ±7	24.1	6.0	18.1
	1/4 - 1/12	1	40 ±15	34.9	2.0	32.9
		2	32 ±9	24.8	4.0	20.8

a. Pipe materials were stainless steel and aluminum for oils but only aluminum for other fluids; all correspond to unmasked cases (t_m = 0).

b. Values of t_r and t_a were calculated from Equations (3) and (4), respectively, using 2 tan ϕ = 16.0 and A = 5.0.

c. M_2O is a mixture of H_2O and D_2O with Σ_{th} = 1.0 cm^{-1}.

d. Cross sections corrected for loss of contrast due to aluminum wedge.

TABLE III

Calculated Detectability of Masked Fluid Film

Fluid	*Pipe, in.*	*Tilt, sec θ*	t_a, *mils*	t_m, *mils*			t_p, *mils*		
				SS	*Cu*	*Pb*	*SS*	*Cu*	*Pb*
D_2O	9/16 - 3/16	1	18.9	4.9	3.4	0	23.8	22.3	18.9
(Σ_{th} = 0.45 cm^{-1})		2	11.9	9.9	6.8	0	21.8	18.7	11.9
	3/8 - 1/8	1	21.6	3.3	2.3	0	24.9	23.9	21.6
		2	13.6	6.6	4.6	0	20.2	18.2	13.6
	1/4 - 1/2	1	24.5	2.2	1.5	0	26.7	26.0	24.5
		2	15.6	4.4	3.0	0	20.0	18.6	15.6
T_2O	9/16 - 3/16	1	26.6	6.1	4.6	0.6	32.7	31.2	27.2
(Σ_{th} = 0.28 cm^{-1})		2	16.3	12.2	9.2	1.3	28.5	25.5	17.6
	3/8 - 1/8	1	29.5	4.1	3.0	0.4	33.6	32.5	29.9
		2	18.6	8.2	6.1	0.8	26.8	24.7	19.4
	1/4 - 1/12	1	33.6	2.7	2.0	0.3	36.3	35.6	33.9
		2	21.4	5.4	4.1	0.6	26.8	25.5	22.0

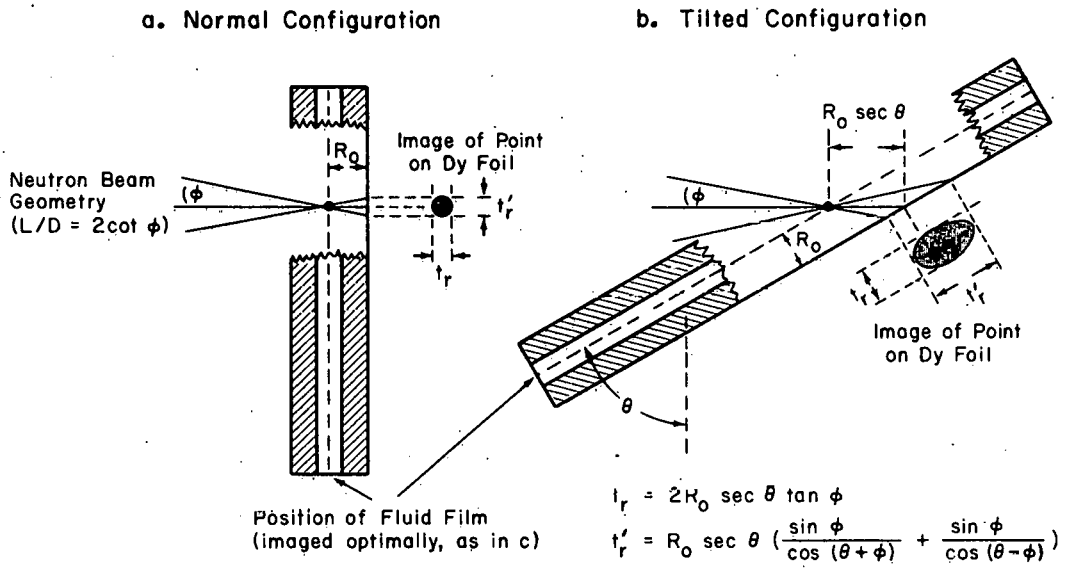

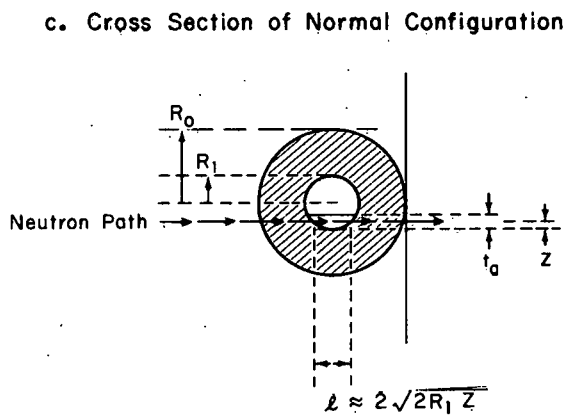

FIGURE 1. Geometry of Fluid Film Detection and Resolution by Neutron Beam.

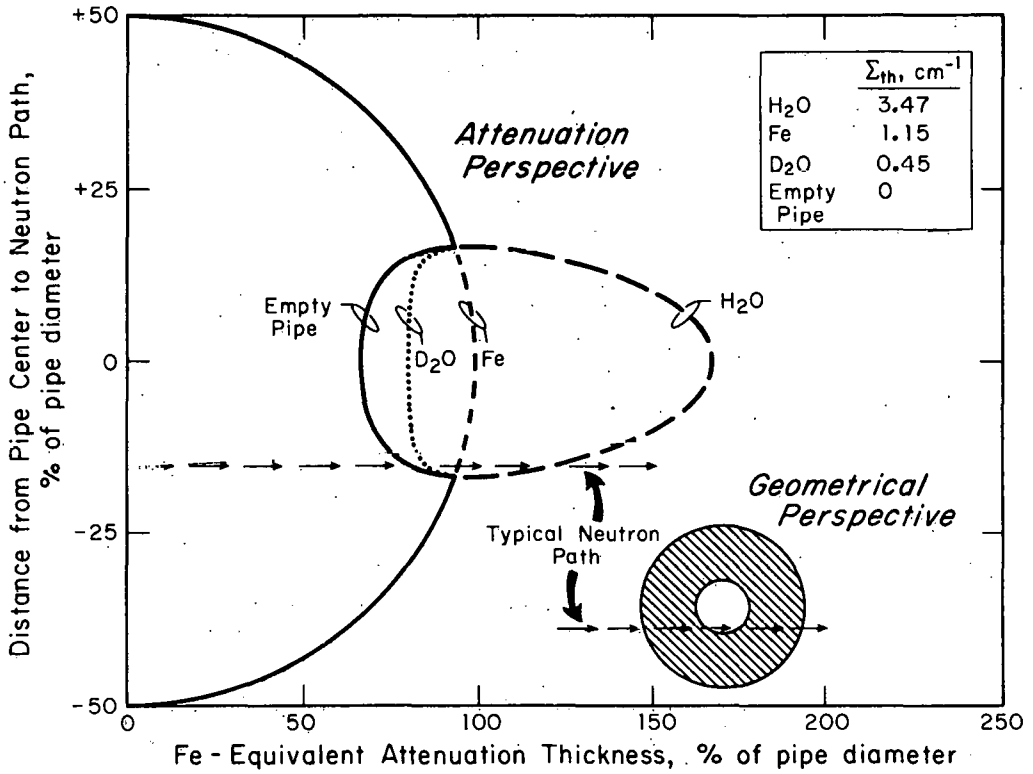

FIGURE 2. Neutron Attenuation of Stainless Steel Pipes containing Various Fluids. The Fe-equivalent attenuation thickness varies according to the location of the traversing neutron path and has the effect of masking weakly attenuating fluids near the tangent edge of the pipe cavity (as represented by the neutron path in the figure).

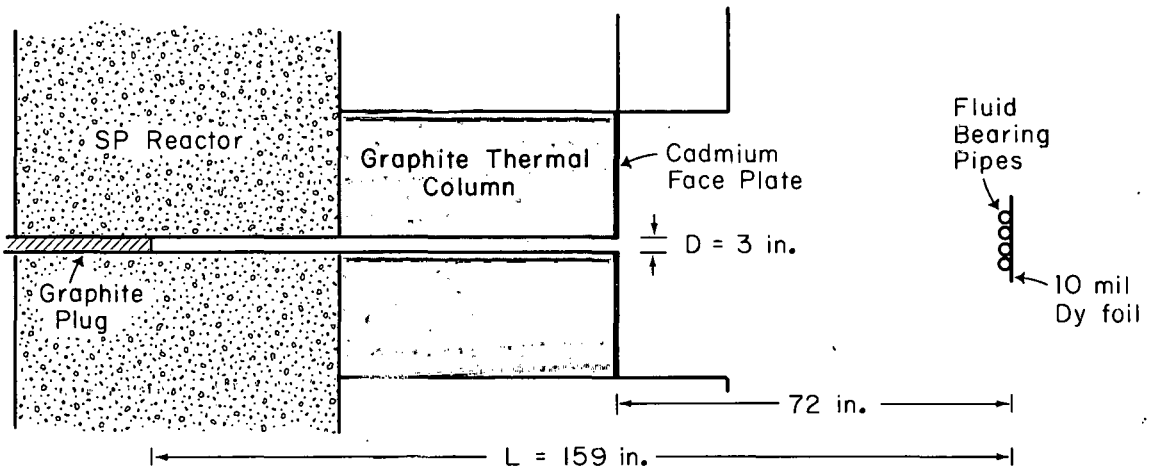

FIGURE 3. Experimental Facility for Producing Neutron Radiographs.

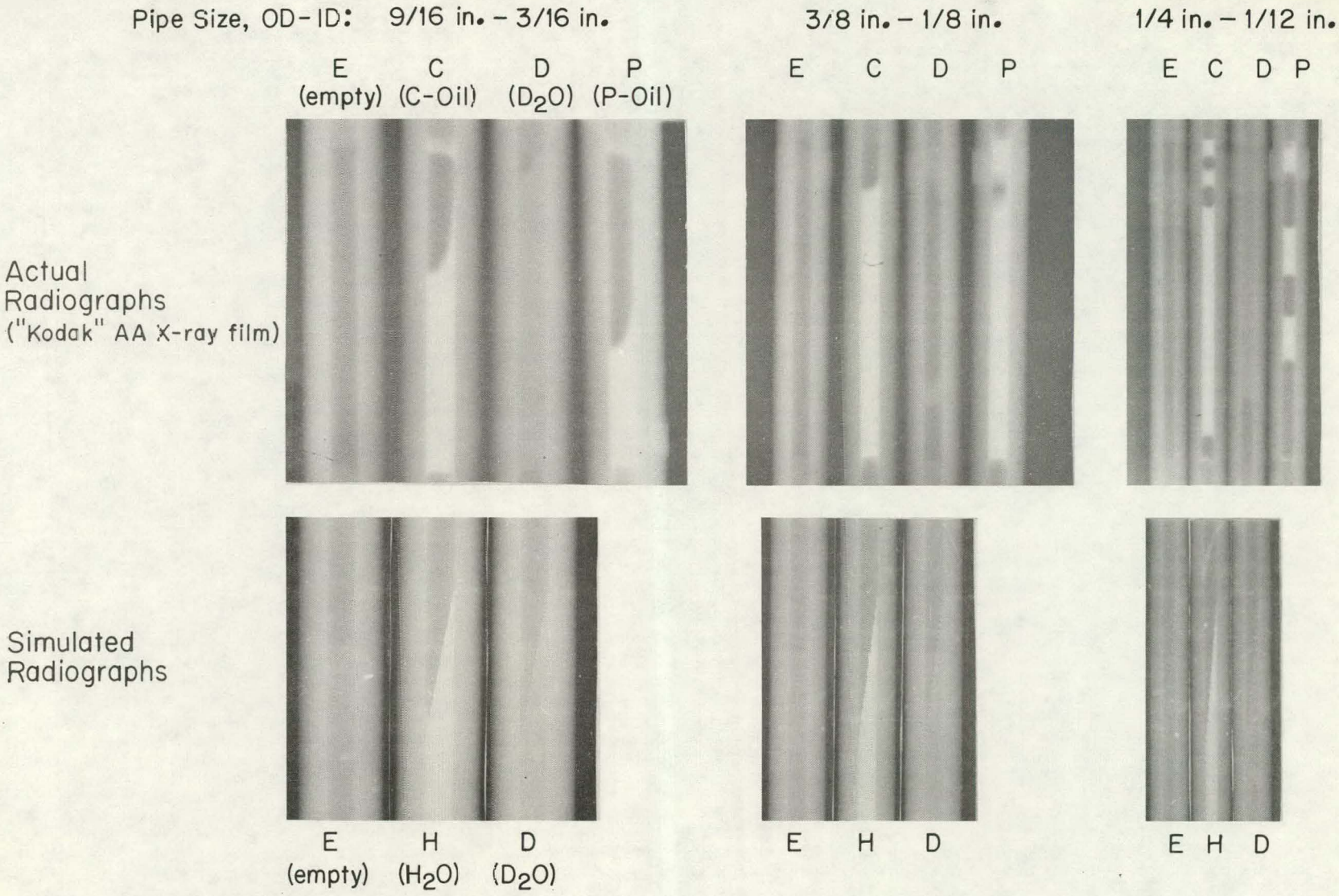

FIGURE 4. Radiographs of Natural (random) Fluid Films in Stainless Steel Pipes Compared with Simulated Radiographs of Trough-Like Films. The oils in the actual radiographs are similar to H_2O in attenuation (refer to Table I for oil specification).

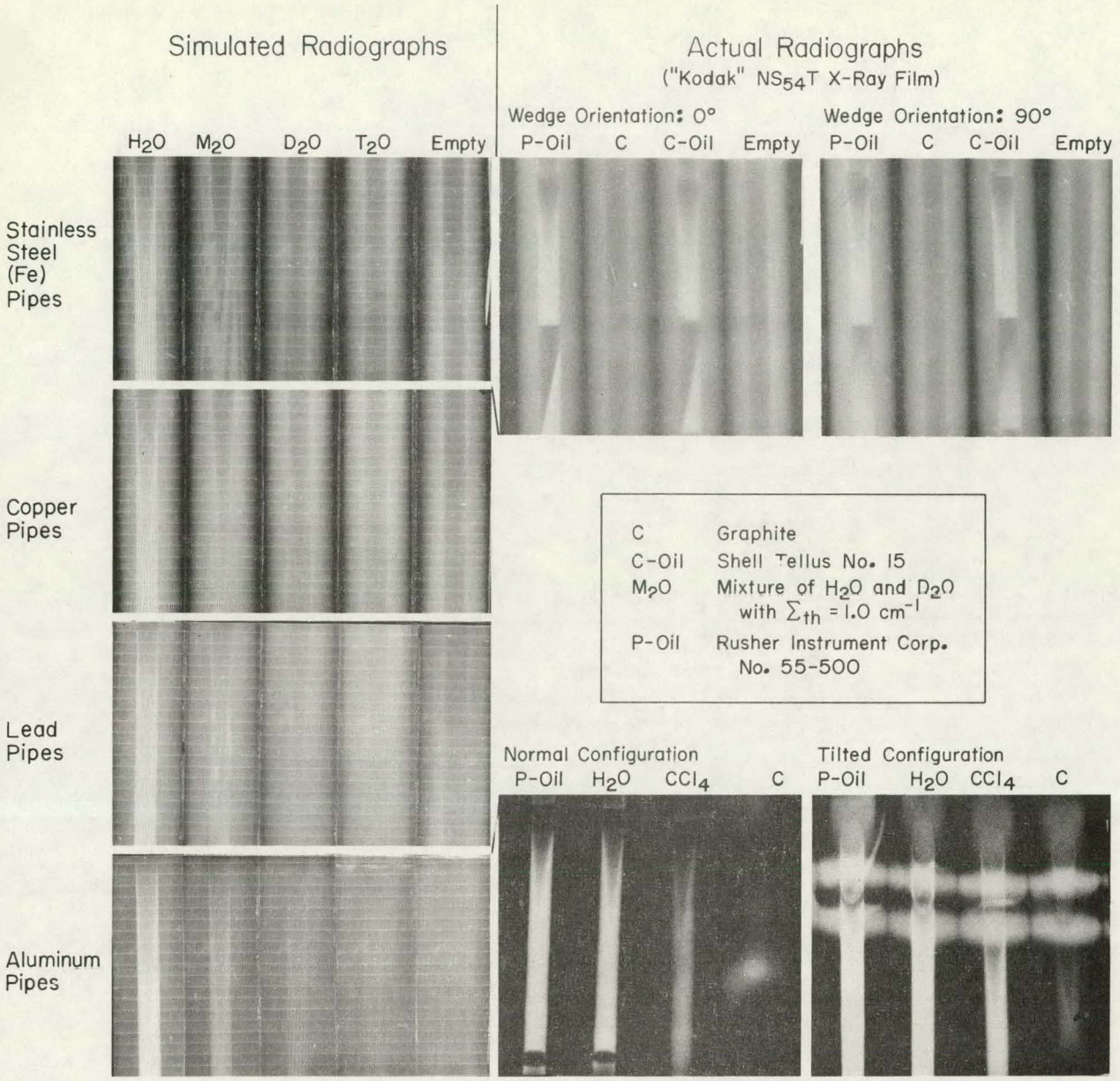

FIGURE 5. Actual and Simulated Radiographs of Fluid Films Defined by Aluminum Wedges in 9/16 in. - 3/16 in. Pipes. The horizontal white lines in the simulations divide regions of constant circular fluid film thickness; the film thickness increases uniformly from zero at the top of each simulation to maximum at the bottom. Respective simulations with H_2O, M_2O, and T_2O are comparable to actual radiographs of oils, CCl_4, and C. The obstruction in the tilted radiograph of aluminum pipes was caused by part of the pipe support mechanism which was also tilted into the neutron beam. (The bright spot on the radiograph for the non-tilted aluminum pipe radiograph of C was probably caused by an oil spot on the Dy foil.)

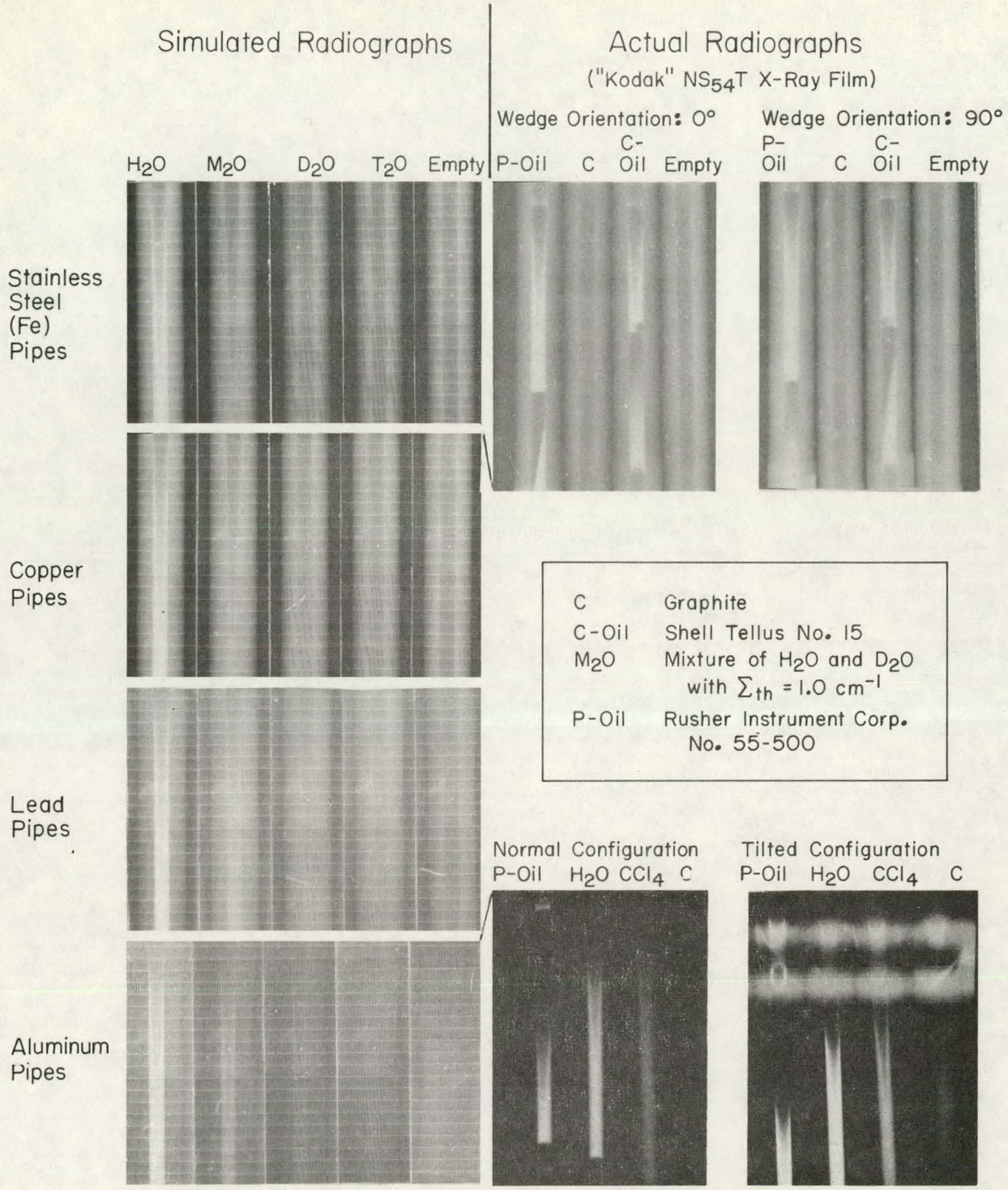

FIGURE 6. Actual and Simulated Radiographs of Fluid Films Defined by Aluminum Wedges in 3/8 in. - 1/8 in. Pipes. (See Figure 5 for general comments.)

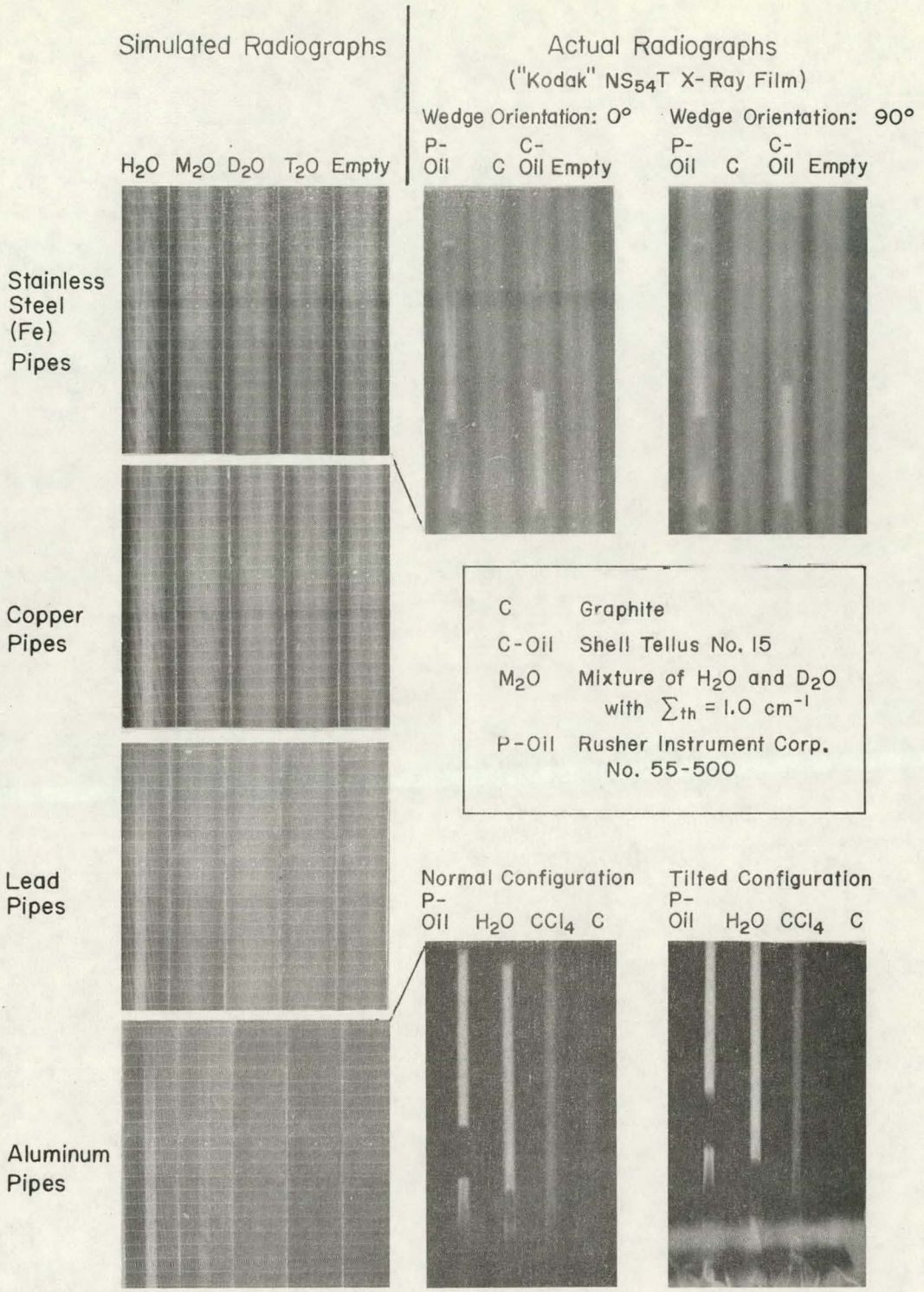

FIGURE 7. Actual and Simulated Radiographs of Fluid Films Defined by Aluminum Wedges in 1/4 in. - 1/12 in. Pipes. (See Figure 5 for general comments.)

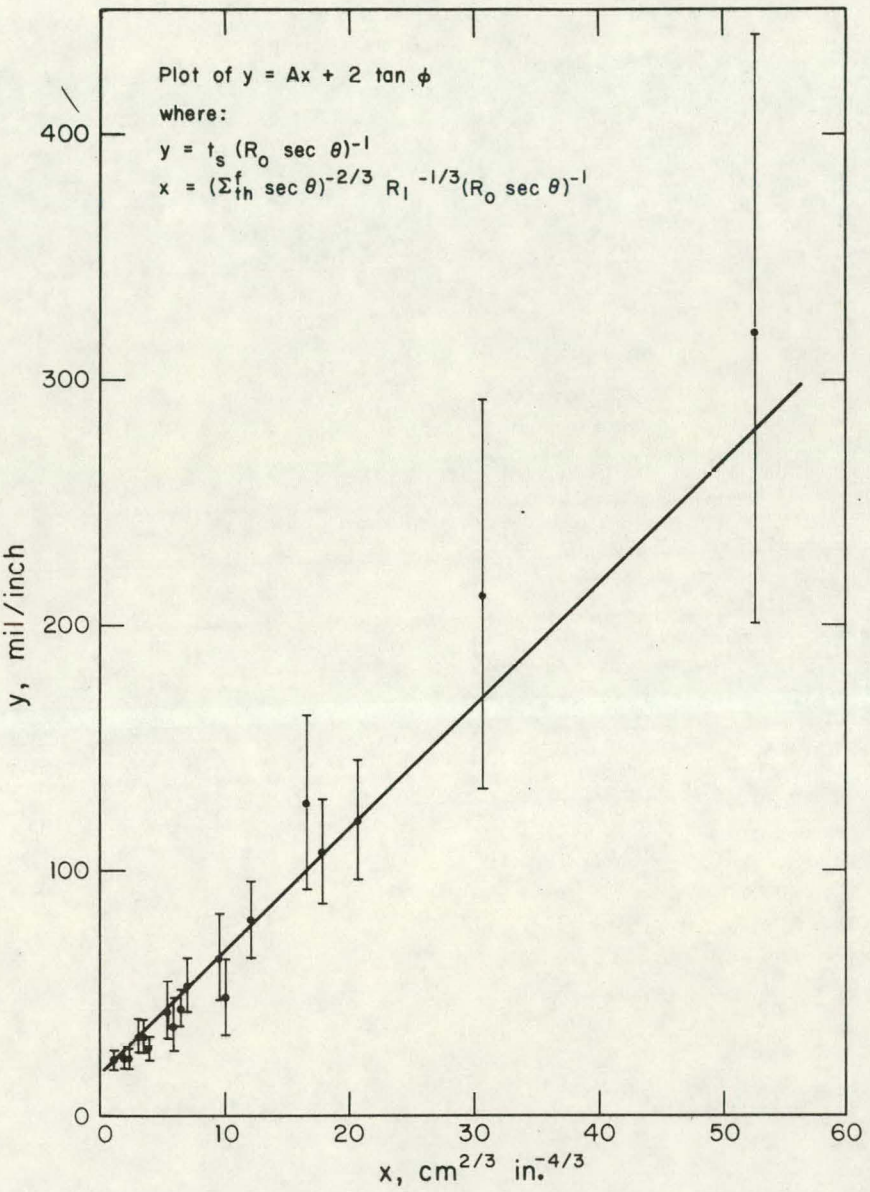

FIGURE 8. Self-Consistency of Model for t_s. The straight line corresponds to 2 tan ϕ = 16.0 mil/in. and A = 5.0 mil $cm^{-2/3}$ $in.^{+1/3}$.

OD-ID, inches:	9/16 - 3/16			3/8 - 1/8			1/4 - 1/12		
Pipe Tilt, sec θ:	1	2	3	1	2	3	1	2	3
Radiographs of T_2O in Stainless Steel Pipes (Simulated)	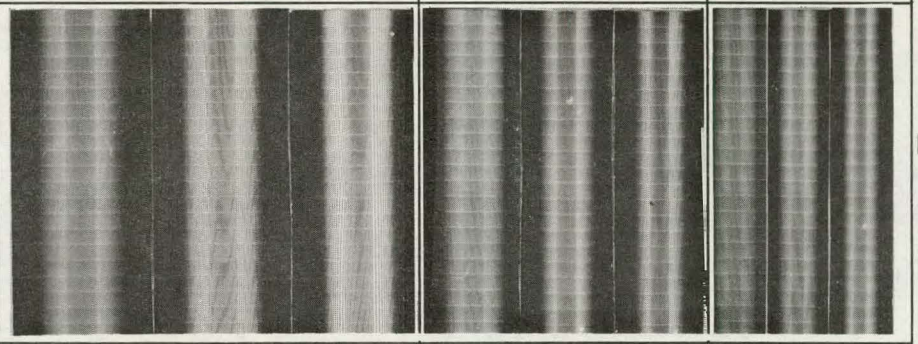								
$\Delta t(\theta)/\Delta t(0°)$:	1.0	6.0	27	1.0	4.1	13	1.0	3.3	7.9
$J_{th}\Delta t$ (relative):	6.0	35.6	160	4.2	17.2	53.5	3.3	11	26

OD-ID, in.:	9/16 - 3/16			3/8 - 1/8			1/4 - 1/12		
Pipe Tilt, sec θ:	1	2	3	1	2	3	1	2	3
Radiographs of T_2O in Aluminum Pipes (Simulated)	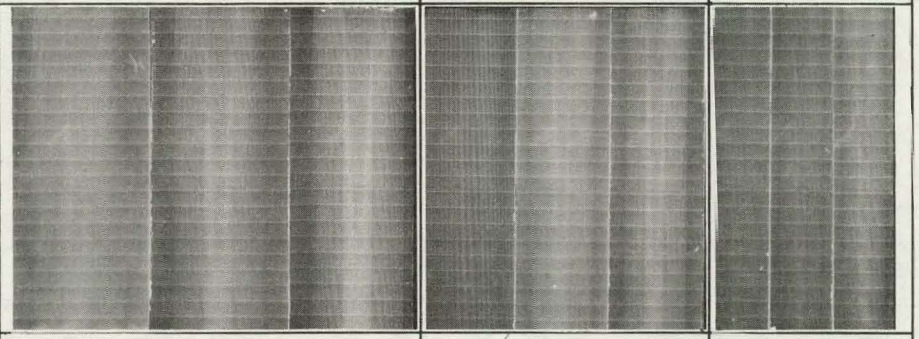								
$\Delta t(\theta)/\Delta t(0°)$:	1.0	2.2	3.6	1.0	2.1	3.4	1.0	2.1	3.3
$J_{th}\Delta t$ (relative):	2.2	4.8	8.0	2.1	4.5	7.2	2.1	4.4	6.8

Neutron Fluence ($J_{th}\ \Delta t$) Considerations

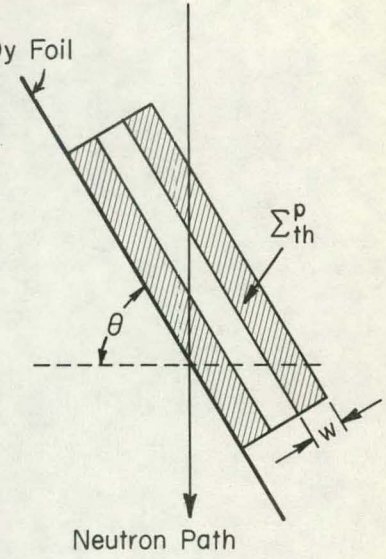

Attenuation by pipe = $\exp(-2w\Sigma^{th}_p \sec\theta)$

Decrease due to foil angle θ = $\cos\theta$

FIGURE 9. Simulated Neutron Radiographs of Annular T_2O Films in Stainless Steel and Aluminum Pipes Tilted Toward the Neutron Beam. Utilizing the neutron fluence consideration described, the relative fluence (exposure time) requirements were calculated as $J_{th}\ \Delta t = \sec\theta \exp(2w\Sigma^p_{th}\sec\theta)$. Values of $\Delta t(\theta)/\Delta t(0°)$ indicate the factor by which exposure times must be increased beyond that of the untilted cases.

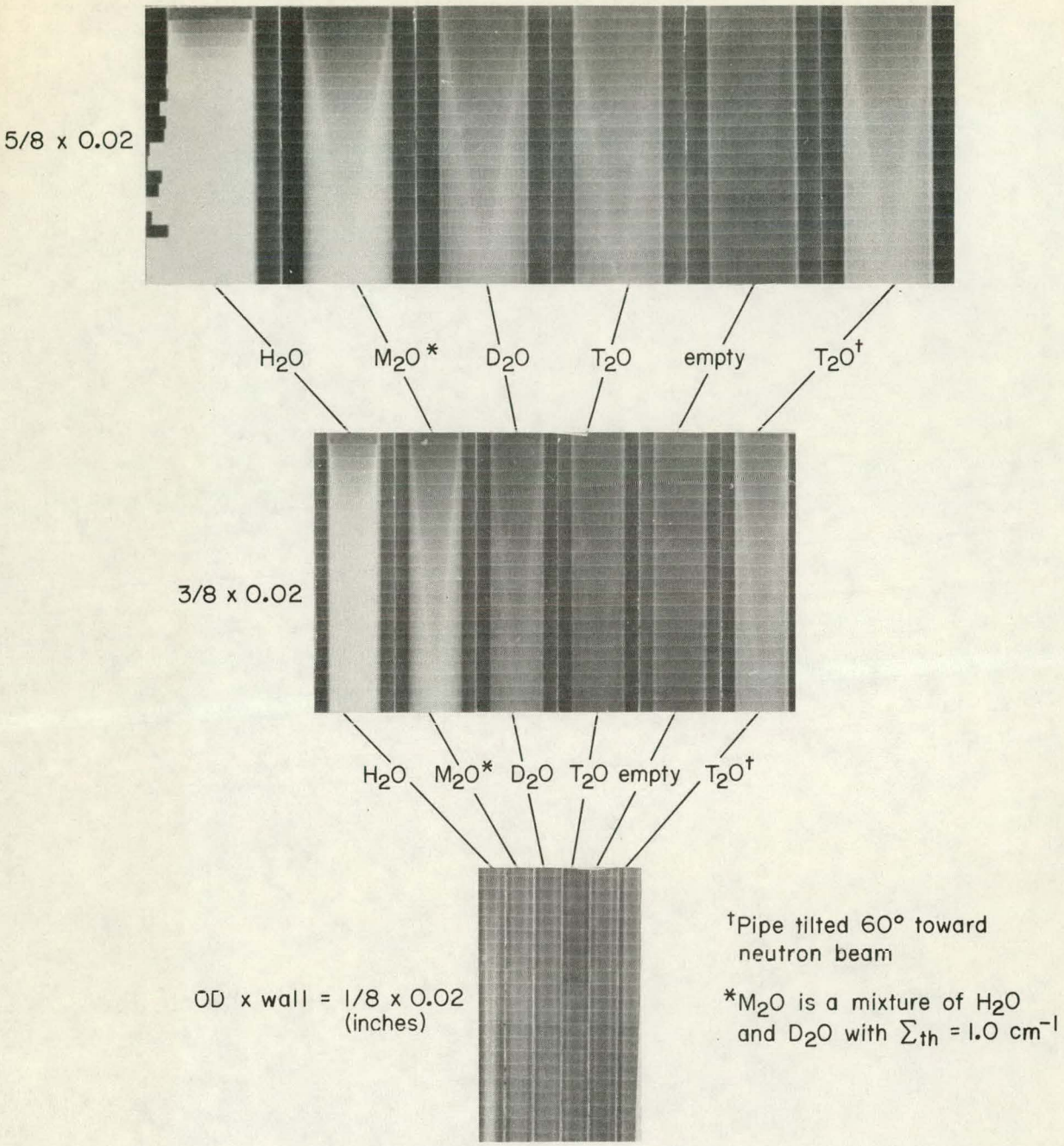

FIGURE 10. Simulated Neutron Radiographs of Various Annular Fluid Films in Thin-Walled Stainless Steel Pipe. (Simulated radiograph of H_2O in 5/8 x 0.02 pipe is jagged on left side due to nature of line spacing routine of simulation code.)